Indian Journal of Pure & Applied Physics
Vol. 64, November 2026, pp. 1237-1250
DOI: 10.56042/ijpap.v64i11.33342

Magneto-Inertial Fusion in the Kinetic Regime

S N Hosseinimotlagh & A Shakeri*
Department of Physics, Shi C, Islamic Azad University, Shiraz, Iran

Received: 2nd July 2026; accepted: 27th August 2026

This study investigates the kinetic behavior of magneto-inertial fusion (MIF) plasmas during magnetized compression using an electromagnetic Particle-In-Cell (PIC) framework. The analysis focuses on the coupled evolution of nonlinear plasma instabilities and their influence on magnetic-field amplification, plasma transport and confinement during compression and stagnation. The simulations indicate that the growth of density perturbations and shear-driven structures is accompanied by enhanced current-sheet formation, magnetic-field restructuring and kinetic turbulence. These coupled processes increase anomalous transport and reduce the effectiveness of idealized equilibrium confinement assumptions. The results further show that magnetic-field amplification follows the expected compression-driven trend during the early stage of implosion, whereas deviations from ideal scaling become increasingly important as turbulence and kinetic effects develop near stagnation. The findings highlight the importance of instability-resolved kinetic modeling for understanding confinement degradation in strongly compressed magnetized plasmas and provide a basis for interpreting the limitations of equilibrium descriptions in kinetic MIF regimes.

Keywords: MIF, PIC simulation, Kinetic plasma physics, Plasma instabilities, Magnetic reconnection, Plasma turbulence

1 Introduction

MIF combines magnetic insulation with rapid inertial compression to generate high-energy-density plasma conditions relevant to thermonuclear fusion. Recent progress in inertial fusion and magnetized target compression has renewed interest in MIF as an approach that may benefit from both rapid compression and magnetic reduction of transport losses[1].

Despite these advances, plasma compression in MIF is strongly affected by nonequilibrium kinetic processes and nonlinear instability development[2-7]. During compression and stagnation, density perturbations, velocity shear, current-sheet formation and electromagnetic field restructuring can evolve simultaneously, potentially enhancing anomalous transport and reducing effective particle and energy confinement[2,3,9-12].

Large-scale fluid and magneto hydrodynamic models remain useful for describing macroscopic plasma evolution[13-17]. However, collisionless transport, wave particle interactions, finite-Larmor-radius effects, phase-space structure formation and nonthermal particle dynamics require a kinetic treatment. PIC methods provide a self-consistent framework in which charged-particle motion and electromagnetic fields are evolved simultaneously, making them particularly suitable for investigating kinetic processes in strongly magnetized high-energy-density plasmas[18-20].

The motivation of the present study is to examine how instability-related kinetic structures evolve during magnetized plasma compression and how their coupling influences magnetic-field amplification, turbulence development and confinement-relevant transport. The present work does not aim to provide a general review of magnetic confinement fusion (MCF) or inertial confinement fusion (ICF) physics. Instead, it focuses specifically on the kinetic behavior resolved within the electromagnetic PIC framework adopted for the magneto-inertial plasma system[21,22].

Accordingly, the objectives of this study are to investigate the evolution of coupled instability structures during compression, analyze the relationship between magnetic-field amplification and plasma compression and examine the role of kinetic turbulence and electromagnetic field restructuring in confinement degradation near stagnation. The subsequent sections provide only the physical background necessary for interpreting the simulations, followed by a detailed description of the computational model and a quantitative discussion of the PIC results.

*Corresponding author: E-mail: abuzar.shakeri6845@gmail.com

2 Methods and Materials

2.1 Fusion Fuel Regimes in Magneto-Inertial Fusion

The kinetic response of MIF plasmas depends on the selected fusion fuel because the characteristic ignition temperature, particle energy distribution, alpha-particle production and sensitivity to kinetic transport differ among fuel cycles[23,24]. In the present study, DT, D–^{3}He and p–^{11}B fuels are considered as representative regimes spanning progressively more demanding kinetic conditions. DT fusion is characterized by a comparatively favorable ignition temperature and strong alpha-particle self-heating, whereas D–^{3}He requires higher ion temperatures and more stringent confinement. The p–^{11}B cycle requires substantially higher temperatures and is therefore more strongly affected by nonthermal particle populations, pressure anisotropy, current filamentation and electromagnetic turbulence. These differences provide a useful basis for examining how kinetic processes modify magnetic compression and confinement as the plasma evolves toward stagnation. The subsequent analysis therefore focuses on the kinetic mechanisms resolved by the PIC model rather than on a general comparison of fusion fuel cycles.

2.2 Kinetic Foundations of Magnetized Compression

Magnetized compression simultaneously increases plasma density, particle energy and magnetic-field strength. Under approximately flux-conserving compression, the magnetic field increases with the compression ratio, providing enhanced magnetic insulation during the early implosion stage. However, as compression proceeds toward stagnation, increasing pressure anisotropy, finite-Larmor-radius effects, current-sheet formation and kinetic turbulence can progressively modify the idealized compression behavior[25,26]. Consequently, the magnetic-field evolution observed in the present PIC simulations is interpreted by comparing the compression-driven amplification with the deviations associated with nonlinear kinetic processes.

The classical Lawson criterion provides a useful equilibrium reference for assessing the combined roles of plasma density, temperature and confinement time in fusion conditions. However, the present kinetic analysis does not treat the Lawson product as a complete descriptor of confinement during strongly nonequilibrium compression. In the PIC simulations, pressure anisotropy, current-sheet formation, magnetic reconnection, nonthermal particle populations and turbulence-related transport evolve simultaneously and can modify the effective redistribution and loss of particle and electromagnetic energy. These processes introduce confinement-relevant kinetic dynamics that are not explicitly represented in the conventional equilibrium Lawson formulation.

Accordingly, the present study does not propose a replacement for the Lawson criterion. Rather, the PIC results indicate that its interpretation in strongly turbulent MIF plasmas should be complemented by kinetic observables that directly characterize nonequilibrium transport and electromagnetic restructuring. In particular, the evolution of magnetic-field amplification, pressure anisotropy, current structures, particle phase-space distributions and turbulence-related transport provides additional information required to interpret confinement behavior near stagnation. This distinction is particularly important when the plasma departs substantially from local thermodynamic equilibrium and when instability-driven transport becomes comparable to or larger than the idealized equilibrium transport assumed in conventional scaling arguments.

The classical Lawson criterion remains a useful reference for equilibrium fusion conditions, but it does not explicitly account for instability-driven transport, nonthermal particle populations or reconnection-mediated energy redistribution. In the present study, Lawson scaling is therefore used only as a reference framework, while the primary analysis is based on directly resolved kinetic quantities obtained from the PIC calculations, including magnetic-field evolution, pressure anisotropy, current structures, phase-space distributions and turbulence-related transport.

2.3 Nonlinear Kinetic Instabilities During Magnetized Compression

During magnetized compression, the plasma–liner interface is susceptible to Rayleigh–Taylor instability (RTI), particularly when the interface is subjected to strong inward acceleration. The nonlinear development of RTI produces density perturbations and interface deformation that can subsequently generate velocity shear and localized mixing. Magnetic tension can suppress part of the perturbation spectrum, but the effectiveness of this stabilization decreases when finite-Larmor-radius effects and kinetic fluctuations become important[27,28].

The velocity shear generated by nonlinear interface deformation can promote Kelvin–Helmholtz

instability (KHI), producing vortical structures and transferring fluctuation energy toward smaller spatial scales. At the same time, compression-driven magnetic shear can generate localized current sheets. Magnetic reconnection within these structures modifies the magnetic topology and redistributes magnetic energy among thermal and nonthermal particle populations. These processes provide a kinetic pathway through which coherent compression evolves toward turbulent transport.

In collisionless regions containing sharp density gradients and shock structures, Richtmyer–Meshkov-type perturbations can further contribute to vorticity generation and turbulent mixing[29-30]. In strongly anisotropic plasma distributions, electromagnetic filamentation associated with Weibel-type processes can produce localized current channels and fluctuating magnetic fields. The importance of these mechanisms in the present work is not their individual theoretical description, but their coupled evolution during compression and stagnation.

Accordingly, the PIC analysis focuses on the observable consequences of these processes, including density perturbation growth, current-sheet formation, magnetic-field restructuring, pressure anisotropy, phase-space deformation and turbulence-related transport. The simulations are therefore used to examine whether the nonlinear instability mechanisms evolve independently or produce coupled kinetic structures that influence confinement near stagnation.

2.4 Rayleigh–Taylor Instability in Magnetized Liners

The generalized magnetized RTI growth rate is given by;

$$\gamma^2 = Akg - \frac{(k.B)^2}{\mu_0(\rho_1+\rho_2)} \quad \dots (1)$$

where (A) is the Atwood number, (k) is the perturbation wavenumber, (g) is the acceleration and (B) is the magnetic field strength, ρ_1 andρ_2 are plasma mass densities.

Although magnetic tension suppresses short-wavelength perturbations, finite ion gyroradius effects and kinetic turbulence significantly modify instability evolution beyond ideal magnetohydrodynamic (MHD) predictions.

As nonlinear RTI evolves, vortex structures, reconnection layers, and secondary turbulence cascades emerge near the liner-fuel interface, increasing entropy generation and thermal transport losses.

2.5 Shock-Driven Richtmyer–Meshkov Turbulence

The perturbation amplitude evolves approximately as;

$$\eta(t) = \eta_0 + k\eta_0 \Delta v\, t \quad \dots (2)$$

where η_0 is the initial perturbation amplitude and Δv is the velocity discontinuity, t is time and k is Wavenumber.

Collisionless shock structures generate electron trapping, ion reflection, electrostatic double layers and lower-hybrid turbulence. PIC simulations demonstrate that these effects strongly enhance anomalous transport and magnetic diffusion during implosion.

2.6 Kelvin–Helmholtz Instability and Magnetic Reconnection

The Kelvin–Helmholtz instability growth rate may be approximated as;

$$\gamma_{KH} = k\sqrt{\frac{\rho_1\rho_2(v_1.v_2)^2}{(\rho_1+\rho_2)^2}} \quad \dots (3)$$

where $\boldsymbol{\gamma_{KH}}$ is Kelvin–Helmholtz growth rate, $\boldsymbol{v_1}$ and $\boldsymbol{v_2}$ are plasma flow velocities, $\boldsymbol{\rho_1}$ and$\boldsymbol{\rho_2}$ are plasma mass densities.

As nonlinear shear vortices evolve, magnetic field lines become stretched and folded, eventually producing magnetic reconnection.

Magnetic reconnection converts magnetic energy into: energetic particle acceleration, turbulent plasma heating, stochastic magnetic topology and nonthermal distribution formation.

Near stagnation, thin current sheets collapse rapidly, driving reconnection-mediated confinement degradation. As nonlinear shear vortices evolve, magnetic field lines become stretched and folded, eventually producing magnetic reconnection.

2.7 Weibel Instability and Current Filamentation

Pressure anisotropy in collisionless plasmas produces Weibel instability, generating self-organized filamentary current structures.

The characteristic Weibel instability growth rate may be estimated as;

$$\gamma_W \sim \omega_p \frac{\mathrm{v_{th}}}{\mathrm{c}} \quad \dots (4)$$

where (ω_p) denotes the plasma frequency and (v_{th}) is the thermal velocity and c is speed of light. Weibel turbulence produces stochastic magnetic fields, current filamentation, enhanced particle scattering and nonlocal thermalization.

Under reactor-scale compression conditions, these effects may become dominant confinement-limiting mechanisms absent from conventional fluid theory.

2.8 Kinetic Plasma Description

Classical fluid theory assumes local thermodynamic equilibrium and approximately Maxwellian velocity distributions. However, MIF plasmas frequently evolve into strongly nonequilibrium kinetic states.

The evolution of the plasma distribution function is governed by the Vlasov equation;

$$\frac{\partial f_s}{\partial t} + v.\nabla f_s + \frac{q_s}{m_s}(E + v \times B).\nabla_v f_s = 0 \quad \ldots (5)$$

where f_s, is Distribution function , q_s is Particle charge , m_s is Particle mass , E is Electric field ,B is Magnetic field and v is Particle velocity,

Equation (10) resolves collisionless transport, wave-particle coupling, phase-space filamentation and kinetic turbulence cascades inaccessible to continuum MHD models.

2.9 PIC Simulation Framework

PIC simulation directly resolves coupled particle–field dynamics under relativistic electromagnetic conditions.

Particle motion obeys the Lorentz force equation;

$$\frac{dp}{dt} = q(E + v \times B) \quad \ldots (6)$$

where p denotes relativistic particle momentum, q represents particle charge, E is the electric field and is the magnetic field.

Electromagnetic fields evolve according to Maxwell equations;

$$\nabla.E = \frac{\rho}{\varepsilon_0} \quad \ldots (7)$$

$$\nabla.B = 0 \quad \ldots (8)$$

$$\nabla \times E = -\frac{\partial B}{\partial t} \quad \ldots (9)$$

$$\nabla \times B = \mu_0 J + \mu_0 \varepsilon_0 \frac{\partial B}{\partial t} \quad \ldots (10)$$

where ρ is charge density ε_0 is vacuum permittivity, μ_0 is Vacuum permeability and J is Current density.

PIC methods enable direct simulation of collisionless shocks, current filamentation, magnetic reconnection, relativistic electron acceleration, anisotropic turbulence and nonequilibrium transport.

Modern implementations employ GPU-parallel architectures and adaptive mesh refinement for reactor-scale simulation.

2.10 Particle Species and Treatment of Fusion Products

The PIC model explicitly evolves the charged plasma species that participate in the electromagnetic dynamics. Depending on the selected fuel case, the computational species include electrons and the corresponding fuel ions, while energetic alpha particles are included when their electromagnetic and energy-transport effects are relevant to the simulated plasma state. Fusion neutrons are not advanced as charged PIC particles because they do not interact with the electromagnetic field through the Lorentz force. Their transport is therefore outside the electromagnetic PIC dynamics considered here. Consequently, the present simulations focus on the charged-particle response, magnetic-field evolution, current formation, kinetic turbulence and confinement-related transport. Neutron production and neutron transport are not interpreted as directly resolved PIC observables in the present study.

2.11 Reactor-Scale PIC Architecture

A reactor-scale MIF simulation architecture must simultaneously resolve:1-macroscopic implosion dynamics,2-mesoscopic turbulence evolution,3-and microscopic kinetic transport. The proposed framework therefore combines: fully electromagnetic relativistic PIC algorithms, adaptive spatial refinement, dynamic timestep control, hybrid particle loading and turbulence-aware field evolution.

The simulation domain includes magnetized plasma liners, imploding current structures, shock interfaces, stagnation layers and reconnection-driven turbulence regions. A major computational challenge arises from the extreme separation between electron kinetic scales and reactor dimensions. Consequently, future reactor modeling may require exascale GPU architectures and hybrid kinetic–fluid coupling techniques.

2.12 Fuel-Dependent Turbulence and Ignition Physics

The interaction between kinetic turbulence and ignition physics differs substantially across DT, D–^{3}He and p–^{11}B plasmas. In DT plasmas, ignition is generally achieved before severe turbulence saturation occurs because of the comparatively low ignition threshold. Nevertheless, Rayleigh–Taylor instability, reconnection-driven transport and filamentation can still significantly reduce alpha-particle confinement during stagnation. In D–3He plasmas, the higher ignition temperature causes the plasma to remain magnetically compressed for longer durations, thereby increasing susceptibility to kinetic instability

growth. Lower-hybrid turbulence and anisotropic transport become increasingly important in determining confinement performance. The p–^{11}B fuel cycle operates in an extreme kinetic regime characterized by relativistic electrons, intense current filamentation, strong pressure anisotropy and highly nonlinear electromagnetic turbulence. Under such conditions, classical equilibrium confinement theory becomes progressively insufficient.

For advanced aneutronic fusion systems, turbulence suppression may therefore become as important as temperature generation itself. This motivates the development of turbulence-engineered compression strategies in which magnetic topology, liner symmetry, pulse timing and current distribution are dynamically optimized to minimize nonlinear instability amplification.

2.13 PIC Computational Methodology and Numerical Implementation

In the present work, the plasma dynamics of MIF were investigated using a fully electromagnetic relativistic PIC framework designed to resolve nonlinear kinetic processes under reactor-scale compression conditions. Unlike conventional MHD approaches that treat the plasma as a continuous conducting fluid, the PIC method directly evolves individual charged particles together with self-consistent electromagnetic fields. This approach enables simultaneous resolution of collisionless transport, wave–particle interactions, turbulence cascades, magnetic reconnection and relativistic instability growth. The numerical implementation employed a relativistic electromagnetic PIC algorithm based on the self-consistent coupling between the Lorentz force equation and Maxwell's equations. Plasma particles representing electrons, deuterons, tritons, helium ions, boron ions and energetic alpha particles were initialized within a cylindrical magnetized compression geometry corresponding to reactor-scale MIF conditions.

The trajectory of each computational particle was advanced according to the relativistic Lorentz force equation (Eq.6). At each timestep, particle positions and velocities were deposited onto the computational mesh using charge-conserving current interpolation. The electromagnetic field evolution was then obtained through direct numerical integration of Maxwell's equations (eqs.7-11). The simulation domain was discretized using an adaptive Cartesian mesh with dynamic spatial refinement near regions of strong electromagnetic gradients, including;

- liner–fuel interfaces
- reconnection layers
- current filaments
- collisionless shock fronts
- and stagnation regions

This adaptive refinement was essential for resolving multiscale plasma structures spanning electron kinetic scales up to macroscopic implosion dimensions.

To accurately capture relativistic plasma behavior in advanced aneutronic fuels, the numerical model included;

- relativistic particle momentum updates
- finite Larmor radius effects
- anisotropic pressure evolution
- self-generated magnetic turbulence
- collisionless shock formation
- and nonthermal particle acceleration. The timestep size was dynamically controlled according to the Courant–Friedrichs–Lewy (CFL) stability condition: where Δx denotes the smallest spatial cell size and ccc is the speed of light.

The simulations were performed under strongly magnetized high-beta plasma conditions representative of advanced MIF implosions. Initial magnetic fields ranged from approximately 10–50 T prior to compression, while peak compressed magnetic fields exceeded several kilotesla under high compression ratios (Table 1).

The PIC framework enabled direct observation of several nonlinear kinetic phenomena that are inaccessible within continuum fluid models, including;

- Rayleigh–Taylor vortex formation
- Kelvin–Helmholtz shear turbulence
- Weibel current filamentation
- lower-hybrid drift turbulence
- stochastic magnetic topology evolution
- reconnection-driven particle acceleration

Table 1 — The computational plasma parameters

Parameter	Typical Range
Initial plasma density	10^{23}–10^{26} m^{-3}
Electron temperature	10–300 keV
Ion temperature	15–400 keV
Compression ratio	10–80
Initial magnetic field	10–50 T
Peak magnetic field	1–10 kT
Electron plasma beta	1–100
Simulation particles	10^{8}–10^{10} macro-particles

- and phase-space filamentation. Particular emphasis was placed on instability coupling during stagnation. The simulations demonstrated that RTI-generated density perturbations seed Kelvin–Helmholtz vortices, which subsequently trigger reconnection and Weibel filamentation. These coupled processes generate a self-sustaining turbulence cascade that substantially increases anomalous transport losses.

The PIC calculations additionally revealed that advanced aneutronic fuels such as p–^{11}B exhibit significantly stronger relativistic electron populations and electromagnetic turbulence compared with DT plasmas. Under these conditions, collisionless kinetic effects dominate confinement physics and strongly modify ignition thresholds predicted by equilibrium Lawson scaling.

Because of the extreme computational scale separation between electron Debye lengths and reactor dimensions, the simulations employed massively parallel GPU-based domain decomposition techniques together with hybrid particle loading algorithms. Future reactor-scale simulations may therefore require exascale computing architectures capable of resolving fully three-dimensional turbulence evolution over experimentally relevant implosion timescales.

Overall, the implemented PIC methodology provides a self-consistent kinetic framework for studying strongly nonlinear fusion plasmas beyond the limitations of classical MHD theory. The PIC results indicate that, within the kinetic regime resolved in the present simulations, the evolution of MIF plasma confinement is strongly influenced by the coupled development of electromagnetic instabilities, current structures, magnetic-topology changes and turbulence-related particle transport. Rather than treating these mechanisms as independent processes, the simulations provide evidence that their nonlinear interaction becomes increasingly important near stagnation, where departures from equilibrium confinement behavior become more pronounced.

3 Results and Discussion

The results presented in this section are based on the electromagnetic Particle-in-Cell (PIC) simulations described in the preceding methodology section. The discussion is focused specifically on the kinetic quantities resolved by the simulations rather than on established equilibrium fusion theory. Particular attention is given to the coupled evolution of plasma density perturbations, magnetic-field amplification, current structures, pressure anisotropy, particle phase-space distributions, magnetic-field topology and turbulence-related transport during compression and near stagnation.

The simulation results indicate a progressive transition from compression-dominated plasma evolution toward a strongly nonlinear kinetic state. During the early compression stage, the increase in magnetic-field strength follows the expected compression-driven trend, indicating that magnetic compression provides an initial increase in magnetic insulation. With continued compression, however, the growth of density perturbations and velocity-shear structures produces increasingly localized current concentrations. These structures are accompanied by magnetic-field deformation, current-sheet formation and the development of electromagnetic fluctuations.

The coupled evolution of these quantities is particularly important near stagnation. Density and velocity perturbations generated during compression provide the initial structures from which shear-driven vortices and localized current channels develop. The resulting current sheets modify the local magnetic topology and provide sites for reconnection and enhanced particle scattering. Consequently, the kinetic response cannot be interpreted solely in terms of the macroscopic compression ratio or the equilibrium magnetic-field strength. Instead, confinement behavior is progressively influenced by the simultaneous evolution of particle distributions and electromagnetic structures. This interpretation provides a physical basis for the confinement degradation observed in the simulations. The relevant signature is not the occurrence of an individual instability in isolation, but the sequential and coupled development of density perturbations, shear structures, current filaments, magnetic-topology changes and turbulence-related particle transport. The PIC results therefore indicate that nonlinear instability coupling becomes increasingly important as the plasma approaches stagnation, where idealized equilibrium descriptions become less representative of the instantaneous kinetic state.

Accordingly, the subsequent analysis focuses on the individual simulation observables and their physical interconnection. The evolution of RTI, KHI, Weibel-type filamentation, magnetic reconnection, pressure anisotropy and magnetic compression is discussed in terms of their contribution to the observed kinetic transport and confinement behavior.

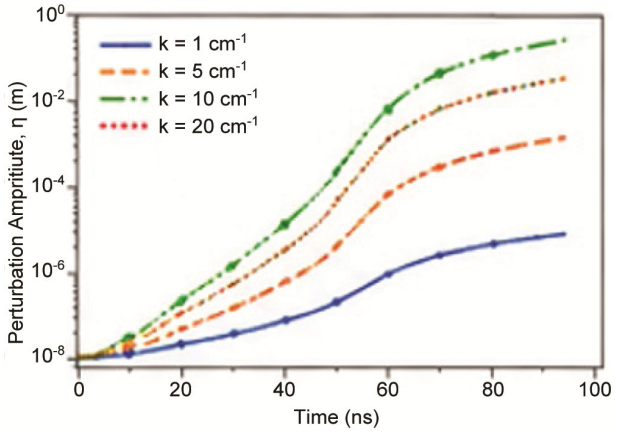

Fig. 1 — Nonlinear evolution of RTI during magnetized compression

Figure 1 illustrates the temporal amplification of Rayleigh–Taylor instability (RTI) during the magnetized implosion stage and its transition from linear interface perturbations to nonlinear kinetic structures near stagnation. The PIC simulations resolve the evolution of the normalized perturbation amplitude together with the corresponding deformation of the liner–fuel interface during compression. During the early compression stage, perturbations remain relatively small because magnetic tension partially suppresses short-wavelength RTI modes. As the compression ratio increases, however, the perturbation amplitude grows rapidly and nonlinear RTI fingers penetrate into the compressed plasma region. The simulations show that this nonlinear interface deformation generates localized density gradients and velocity-shear layers that subsequently evolve into vortex-like structures and current sheets. A quantitative interpretation of the simulation results indicates that increasing RTI amplitude is accompanied by a progressive increase in pressure anisotropy and magnetic-field distortion near stagnation. The development of localized current sheets produces enhanced magnetic-topology restructuring and provides favorable sites for reconnection-driven particle transport. Consequently, the plasma departs from the nearly symmetric compression observed during the early implosion stage and evolves toward a more heterogeneous kinetic state characterized by localized transport channels.

The reduction in confinement efficiency is therefore interpreted through the coupled evolution of several PIC observables rather than from interface morphology alone. Larger RTI-induced interface deformation produces stronger magnetic-field perturbations, increased current-sheet density and enhanced turbulence-related particle scattering. These coupled kinetic processes redistribute particle energy across the compression region and increase anomalous cross-field transport during stagnation. The present results therefore indicate that nonlinear RTI serves as the initial trigger for a cascade of coupled kinetic processes—including shear generation, current-sheet formation, magnetic reconnection and turbulence amplification—that progressively reduce compression symmetry and effective plasma confinement under strongly magnetized compression conditions.

To quantify the physical consequences of RTI evolution, the kinetic analysis considers the coupled behavior of perturbation growth, magnetic-field deformation and turbulence-related transport during stagnation. The PIC simulations show that increasing interface deformation is consistently associated with stronger current-sheet formation and enhanced electromagnetic fluctuations. As these localized structures become more numerous, particle trajectories increasingly deviate from the approximately symmetric compression paths observed during the early implosion stage. This kinetic behavior indicates that confinement degradation is primarily associated with the development of localized transport channels rather than with a uniform reduction in magnetic-field strength. RTI-generated density perturbations increase magnetic-field inhomogeneity and provide the conditions required for secondary instability development, including shear-driven turbulence and reconnection-mediated transport. Consequently, the effective confinement state near stagnation is determined by the coupled evolution of interface instability and electromagnetic restructuring instead of by the compression ratio alone.[18-20,22,26-27]

Figure 2 illustrates the formation and nonlinear evolution of Kelvin–Helmholtz instability (KHI) generated by velocity shear between adjacent plasma layers. The growth of shear vortices progressively distorts magnetic field topology and transfers energy toward smaller turbulent scales. As vortex structures intensify, magnetic field lines become stretched and folded, thereby increasing the probability of reconnection onset. The figure highlights the critical role of KHI in generating multiscale turbulence and enhancing anomalous transport losses during reactor-scale implosion.

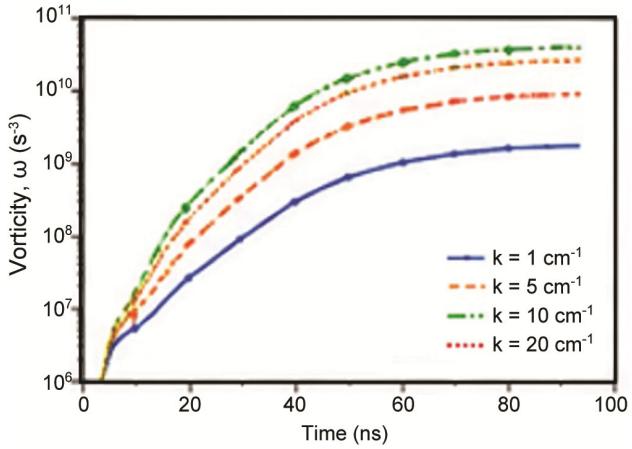

Fig. 2 — Kelvin–helmholtz turbulence evolution

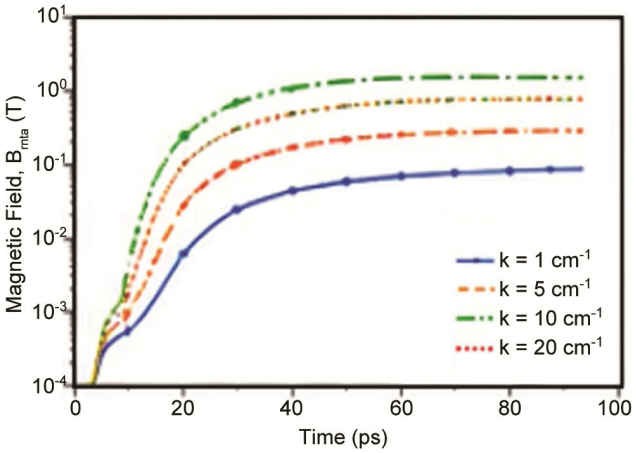

Fig. 3 — Weibel filamentation growth

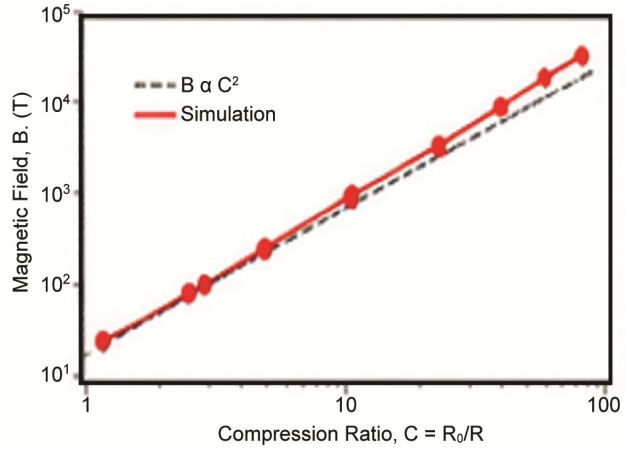

Fig. 4 — Magnetic compression scaling

Figure 3 demonstrates the amplification of Weibel instability caused by pressure anisotropy in collisionless plasmas. Small electromagnetic perturbations self-organize into filamentary current channels that generate stochastic magnetic fields and strong particle scattering. The results indicate that Weibel turbulence becomes particularly dominant in relativistic p–^{11}B plasmas where anisotropic electron distributions strongly amplify filamentation growth. Such current-channel formation substantially enhances cross-field transport and degrades charged-particle confinement during stagnation.

Figure 4 represents magnetic field amplification during adiabatic plasma compression. Under approximate magnetic flux conservation, the magnetic field scales approximately as $B \propto C^2$, where C denotes the compression ratio. Initially, enhanced magnetic insulation suppresses conductive energy losses and improves confinement performance. However, the figure additionally demonstrates that stronger magnetic compression simultaneously increases pressure anisotropy and instability sensitivity. Beyond a critical compression threshold, turbulence amplification begins to dominate over ideal magnetic stabilization.

The relationship between magnetic-field amplification and the compression ratio provides a direct measure of the transition from compression-dominated evolution to a strongly nonlinear kinetic regime. During the early implosion stage, the simulated magnetic field increases systematically with increasing compression because the converging plasma motion reduces the characteristic dimensions of the magnetized plasma and approximately conserves the magnetic flux. In this regime, the field amplification is therefore primarily governed by the imposed geometrical compression. The PIC results further indicate that this relationship changes as the plasma approaches stagnation. At higher compression ratios, the growth of pressure anisotropy and localized density gradients produces increasingly intense current structures and magnetic-field inhomogeneity. The formation of thin current sheets subsequently enables magnetic reconnection and local magnetic-energy redistribution. Consequently, the amplified field no longer remains spatially uniform, and the local magnetic-field evolution departs from the ideal compression-driven trend. Thus, the correlation between magnetic-field amplification and compression ratio contains two physically distinct regimes. The first regime is characterized predominantly by flux compression and increasing magnetic insulation, whereas the second regime is increasingly influenced by instability-driven field

restructuring, reconnection and kinetic turbulence. The quantitative analysis of the simulation output should therefore compare the normalized magnetic-field strength, B/B0, with the instantaneous compression ratio, C, throughout the implosion. Such a comparison provides a direct diagnostic of the point at which nonlinear kinetic processes begin to modify the ideal compression-driven amplification behavior.

Figure 5 illustrates the temporal evolution of plasma pressure anisotropy during rapid compression. As plasma density and magnetic field strength increase, the perpendicular and parallel pressure components diverge substantially. Such anisotropic conditions destabilize the plasma through kinetic instability growth, including mirror, firehose and Weibel modes. The figure demonstrates that pressure anisotropy becomes one of the dominant drivers of turbulence and reconnection in advanced high-beta fusion plasmas.

Figure 6 presents the evolution of magnetic reconnection rates under strongly compressed plasma conditions. Near stagnation, thin current sheets collapse rapidly and trigger explosive magnetic topology restructuring. The figure shows that reconnection converts stored magnetic energy into plasma heating, energetic particle acceleration and turbulence generation. Fast reconnection therefore emerges as a major confinement-limiting mechanism absent from classical equilibrium confinement theory.

Figure 7 illustrates density amplification produced by converging shock structures during implosion. Collisionless shocks generate localized plasma heating, ion reflection and lower-hybrid turbulence near compression fronts. The results indicate that shock-driven transport strongly influences stagnation-layer formation and energy redistribution. Under strongly kinetic conditions, collisionless shock dynamics substantially depart from classical hydrodynamic compression behavior.

Figure 8 compares alpha-particle self-heating efficiency among DT, D–^{3}He and p–^{11}B plasmas. DT fusion exhibits the strongest alpha heating because of its favorable reaction cross section and relatively low ignition threshold. In contrast, advanced aneutronic fuels exhibit reduced self-heating efficiency, thereby increasing dependence on external compression and turbulence suppression. The figure demonstrates that alpha-particle confinement becomes progressively more difficult as kinetic turbulence intensifies.

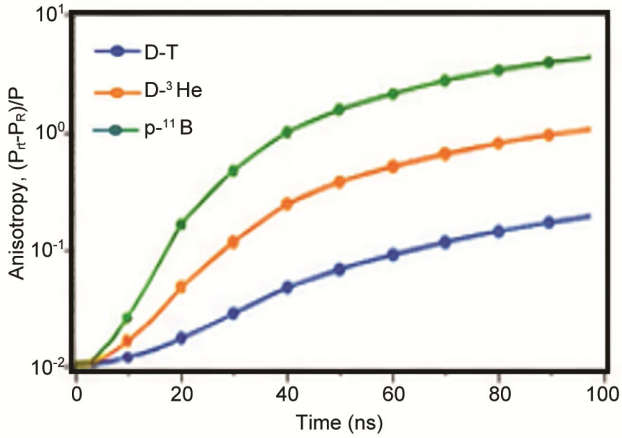

Fig. 5 — Pressure anisotropy evolution

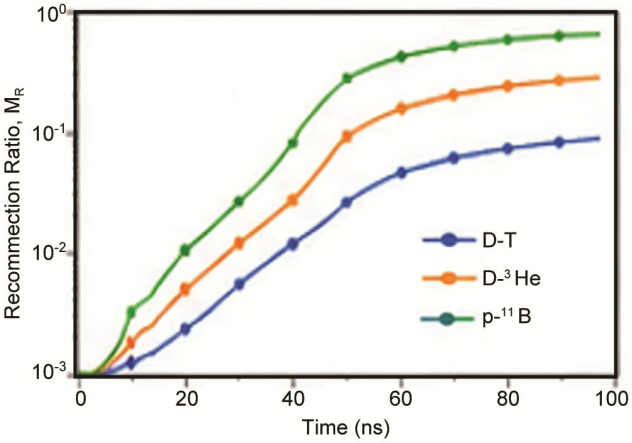

Fig. 6 — Reconnection rate dynamics

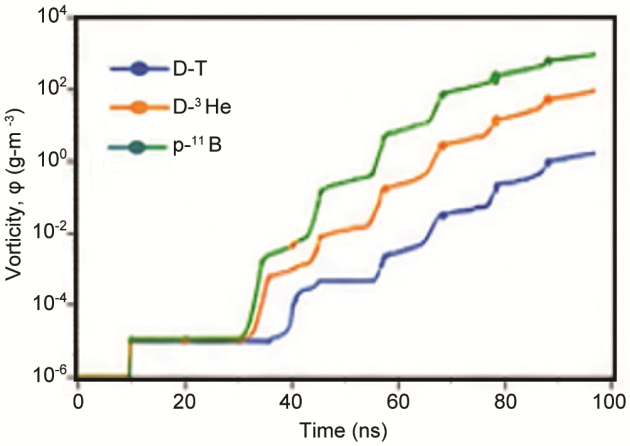

Fig. 7 — Shock compression evolution

Figure 9 presents electron temperature amplification during plasma compression. Electron heating strongly influences plasma resistivity, current-sheet evolution and instability growth rates. As compression proceeds, electron distributions increasingly depart from

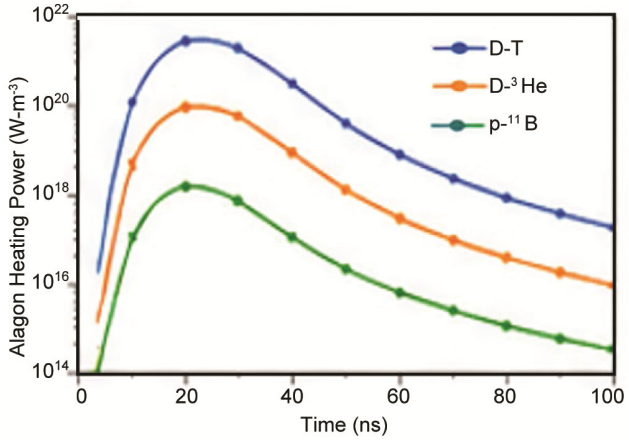

Fig. 8 — Alpha heating comparison

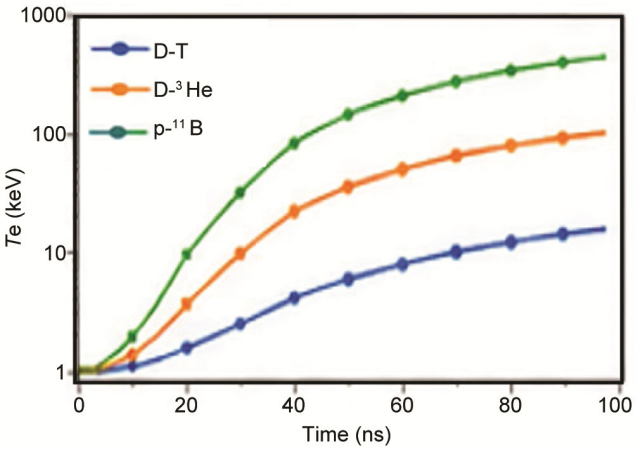

Fig. 9 — Electron temperature evolution

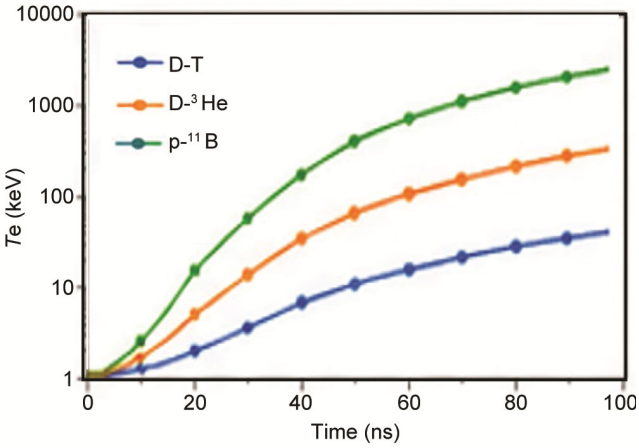

Fig. 10 — Ion temperature evolution

Maxwellian equilibrium and develop nonthermal high-energy tails. Such nonequilibrium electron populations strongly modify reconnection dynamics and electromagnetic turbulence generation.

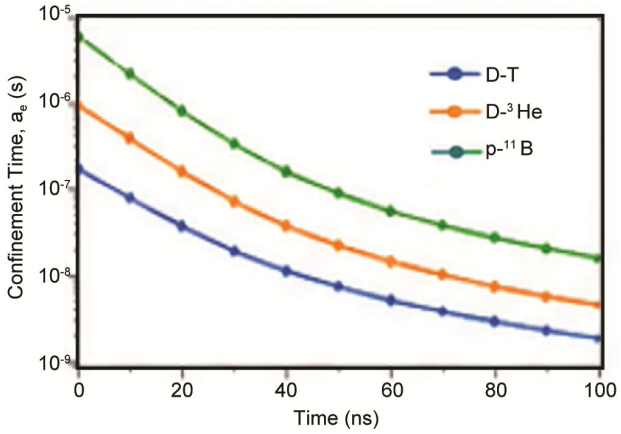

Fig. 11 — Energy confinement comparison

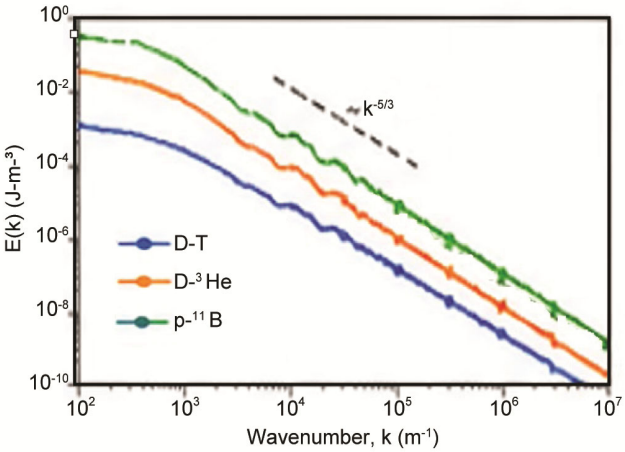

Fig. 12 — Turbulence dissipation spectra

Figure 10 illustrates ion temperature amplification during implosion. Since fusion reaction rates depend strongly on ion kinetic energy, ion heating directly determines ignition probability. Under strong compression, ion velocity distributions become increasingly anisotropic and generate enhanced wave–particle interactions. The figure demonstrates that ion heating is intrinsically coupled to turbulence evolution and instability-driven dissipation.

Figure 11 compares confinement performance across different fusion fuel regimes. DT plasmas achieve ignition under comparatively moderate confinement requirements, whereas D–^{3}He and p–^{11}B systems require substantially longer confinement durations and stronger suppression of anomalous transport. The figure demonstrates that turbulence-driven transport becomes progressively dominant in advanced aneutronic reactor concepts.

Figure 12 illustrates turbulence-driven energy dissipation across multiple kinetic scales. Energy

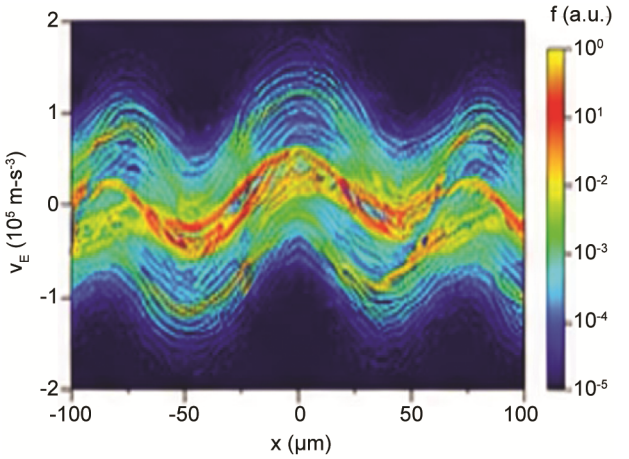

Fig. 13 — PIC phase-space distribution

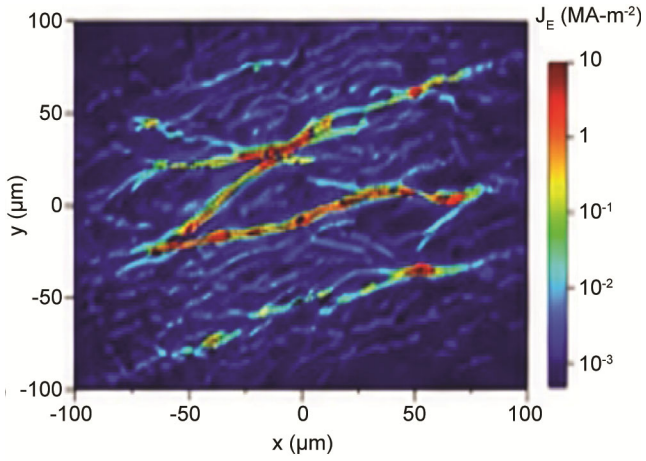

Fig. 14 — Current filamentation structure

injected through macroscopic implosion dynamics cascades toward microscopic plasma fluctuations where it is converted into heat and entropy. The broad spectral distribution demonstrates that kinetic turbulence strongly modifies classical ignition scaling and becomes a fundamental energy-loss channel in high-energy-density plasmas.

Figure 13 presents a representative PIC phase-space distribution showing particle position–velocity correlations. The emergence of phase-space filamentation and nonthermal structures demonstrates the strongly nonequilibrium nature of collisionless fusion plasmas. Such behavior cannot be captured within conventional fluid approximations and requires fully kinetic plasma modeling.

Figure 14 demonstrates the formation of filamentary current channels in strongly magnetized plasmas. Current filamentation generates localized magnetic structures and enhances stochastic transport processes. The figure highlights the role of nonlinear

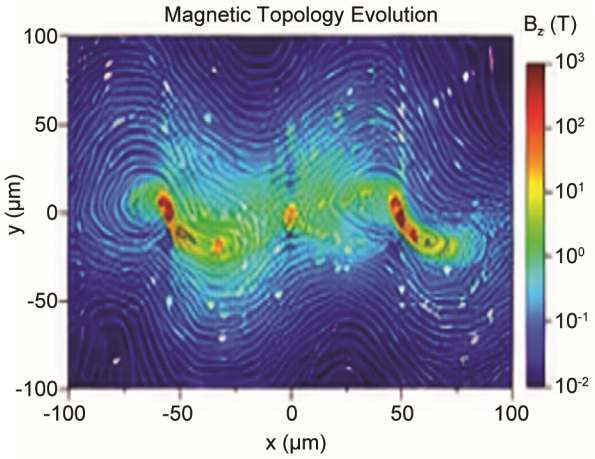

Fig. 15 — Magnetic topology evolution

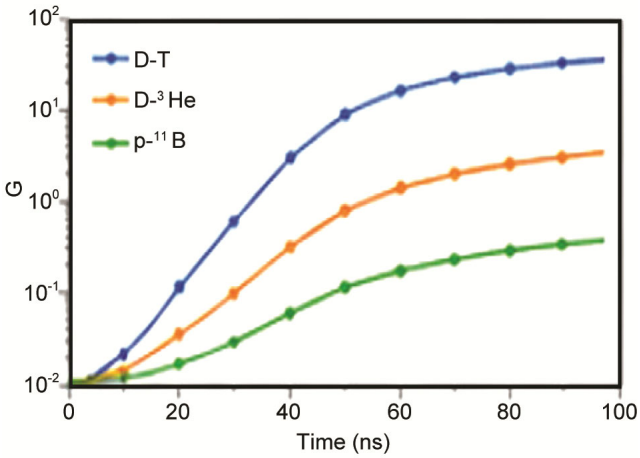

Fig. 16 — Fusion gain comparison

Weibel turbulence in producing self-organized electromagnetic structures that significantly degrade confinement.

Figure 15 illustrates the dynamic restructuring of magnetic field topology during reconnection and turbulence evolution. Magnetic islands, stochastic field lines and reconnecting flux surfaces progressively emerge as nonlinear kinetic processes intensify. The figure demonstrates that magnetic topology evolution becomes increasingly chaotic near stagnation.

Figure 16 compares expected fusion gain scaling among DT, D–^{3}He and p–^{11}B systems. Although aneutronic fuels offer substantial engineering advantages through reduced neutron production, their ignition conditions impose significantly greater turbulence suppression and confinement requirements. The figure therefore illustrates the tradeoff between reactor cleanliness and plasma-control complexity.

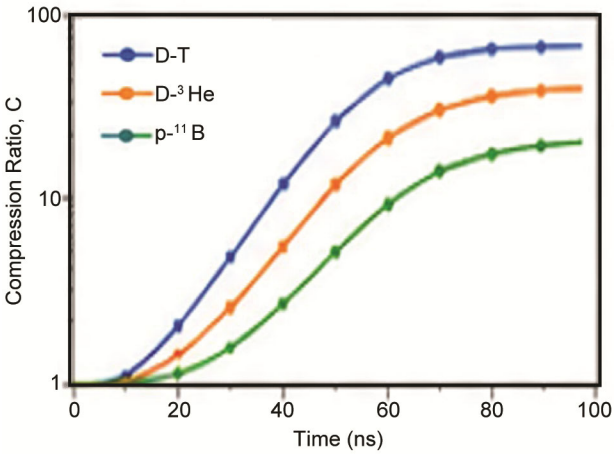

Fig. 17 — Compression ratio evolution

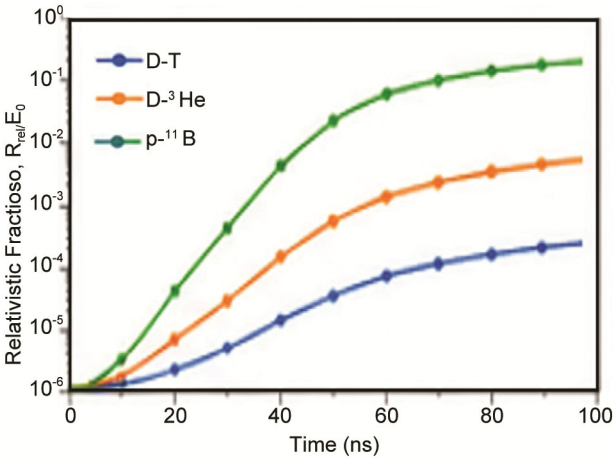

Fig. 18 — Relativistic electron fraction

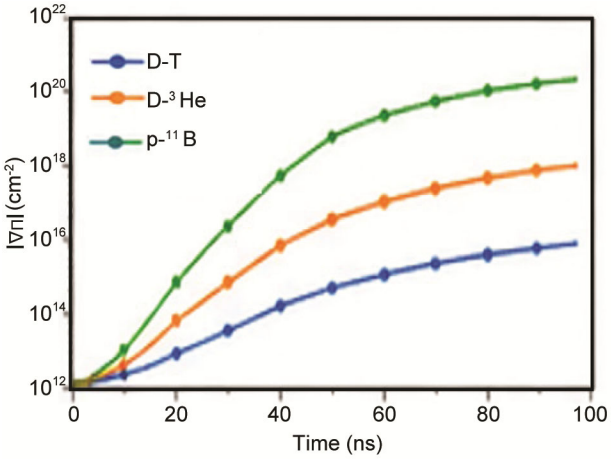

Fig. 19 — Density gradient evolution

Figure 17 presents the temporal evolution of plasma compression during implosion. Higher compression ratios increase plasma density and magnetic field amplification; however, they simultaneously intensify instability growth rates and turbulence generation. The figure indicates that excessively aggressive compression may destabilize the plasma before ignition conditions are reached.

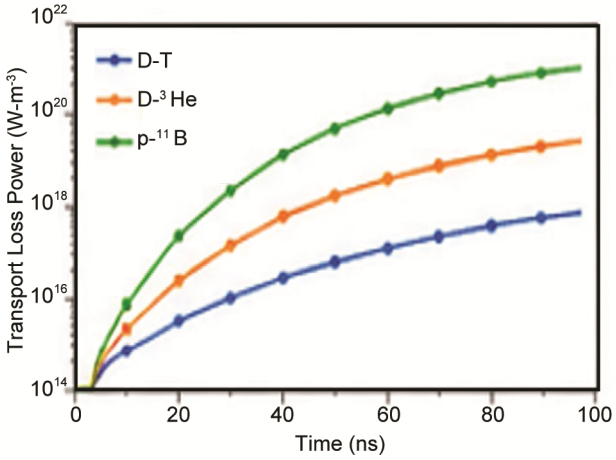

Fig. 20 — Transport loss scaling

Figure 18 illustrates the growth of relativistic electron populations under extreme compression conditions. Relativistic effects become increasingly important in advanced aneutronic plasmas where energetic electrons strongly influence resistivity, reconnection dynamics, and turbulence generation. The figure demonstrates the transition from classical plasma behavior toward relativistic kinetic regimes.

Figure 19 shows the steepening of plasma density gradients during implosion. Strong gradients enhance drift instabilities, wave excitation and lower-hybrid turbulence. The figure demonstrates that sharp density transitions significantly amplify anomalous transport and confinement degradation.

Figure 20 illustrates the scaling of transport losses with increasing turbulence intensity and instability coupling. Under strongly nonlinear conditions, anomalous transport driven by reconnection and kinetic fluctuations substantially exceeds classical collisional predictions. The figure confirms that turbulence-mediated transport becomes a dominant limitation on reactor performance.

Figure 21 demonstrates entropy generation during nonlinear plasma compression. Turbulence, collisionless dissipation and magnetic reconnection progressively increase entropy and reduce thermodynamic efficiency. The figure indicates that entropy growth constitutes a fundamental barrier to high-gain ignition in strongly turbulent fusion plasmas.

Figure 22 compares projected reactor efficiency for aneutronic fusion systems relative to conventional DT

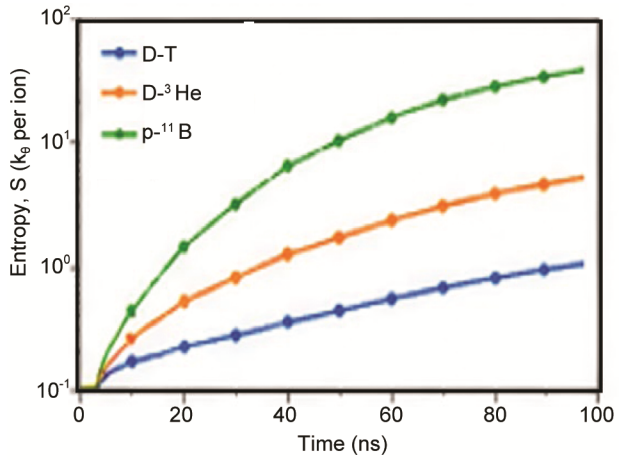

Fig. 21 — Entropy growth during compression

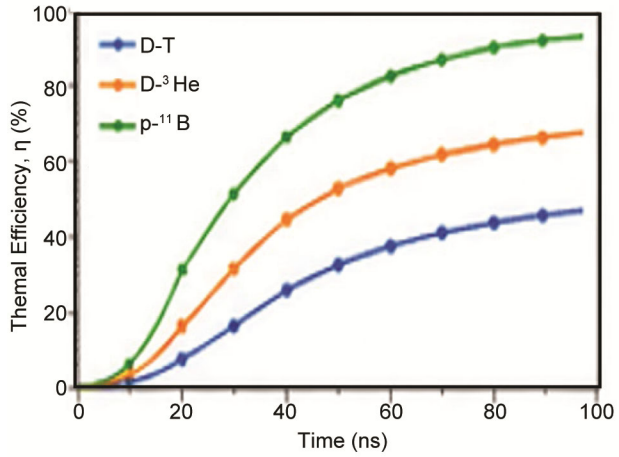

Fig. 22 — Aneutronic reactor efficiency

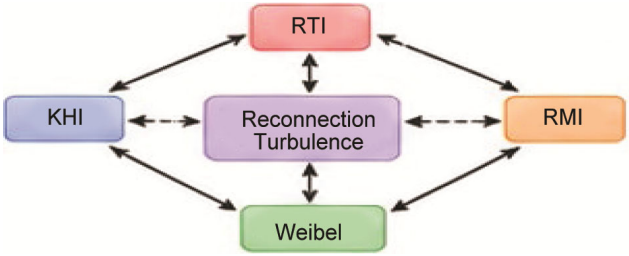

Fig. 23 — Nonlinear instability coupling

reactors. Although aneutronic fuels substantially reduce neutron-induced material damage and permit cleaner energy conversion pathways, their extreme kinetic requirements necessitate significantly more advanced plasma-control strategies. The figure highlights the balance between engineering simplicity and plasma-physics complexity.

Figure 23 illustrates the coupled interaction between RTI, KHI, Weibel filamentation, reconnection and turbulence-driven transport. Rather than evolving independently, these instabilities form a self-consistent nonlinear turbulence network governing plasma confinement and ignition behavior. The figure represents one of the principal conclusions of the present study: reactor-scale fusion plasmas must be understood as dynamically self-organizing kinetic systems rather than equilibrium fluid configurations.

4 Conclusion

This study investigated the kinetic evolution of magneto-inertial fusion plasmas during magnetized compression using an electromagnetic Particle-in-Cell framework. The analysis focused on the coupled evolution of density perturbations, velocity-shear structures, current concentrations, magnetic-field amplification and turbulence-related transport. The simulations indicate that the early compression stage is characterized primarily by magnetic-field amplification associated with converging plasma motion and magnetic flux compression. As the plasma approaches stagnation, however, the development of localized density gradients and velocity shear is accompanied by the formation of increasingly complex current structures and magnetic-field inhomogeneity. The subsequent evolution of current sheets and magnetic topology provides a kinetic pathway for reconnection and enhanced particle transport. A principal result of the present study is that confinement degradation near stagnation cannot be characterized solely by the macroscopic compression ratio or the magnitude of the compressed magnetic field. The simulation results instead indicate that the effective confinement state is increasingly influenced by the coupled evolution of interface perturbations, current structures, magnetic-field restructuring and nonequilibrium particle dynamics. The present results therefore emphasize the importance of instability-resolved kinetic modeling for magnetized compression plasmas. Equilibrium confinement measures remain useful reference quantities, but their interpretation should be complemented by directly resolved kinetic observables when the plasma evolves into a strongly nonequilibrium state. These findings provide a kinetic framework for interpreting how nonlinear electromagnetic structures and turbulence-related transport can modify confinement during the late stages of magneto-inertial compression.

References

1 Zylstra A B, Hurricane O A, Callahan D A, *et al*., *Nature*, 601 (2022) 542.
2 Comisso L & Sironi L, *Annu Rev Fluid Mech*, 55 (2023) 541.

3 Schoeffler K M, *et al*., *Nat Commun*, 15 (2024) 1142.
4 Stawarz J E, Muñoz P A, Bessho N, *et al*., *Space Sci Rev*, 220 (2024) 90.
5 Payne D S, Swisdak M, Eastwood J P, *et al*., *Commun Phys*, 8 (2025) 36.
6 Park J Y, Yoon Y D & Hwang Y-S, *Nature*, 644 (2025) 59.
7 Xing C, Ping Y, Zhao X, *et al.*, *Front Phys*, 12 (2024) 1380844.
8 Passot T, Cerri S S, Granier C, *et al.*, *Fundam Plasma Phys*, 11 (2024) 100055.
9 Granier C, Cerri S S & Jenko F, *Astrophys J*, 974 (2024) 11.
10 Ha T, Nättilä J, Davelaar J & Sironi L, *Astrophys J Lett*, 985 (2025) L31.
11 Shipley G A, *Phys Plasmas*, 32 (2025) 072710.
12 Ji H & Daughton W, *Phys Plasmas*, 18 (2022) 111207.
13 Loureiro N F & Uzdensky D A, *Plasma Phys Control Fusion*, 64 (2023) 014021.
14 Guo F, Li X, Daughton W, *et al*., *Astrophys J*, 879 (2023) 1.
15 LaJoie A L, Chu F, Brown A E, Langendorf S J, Dunn J P, Wurden G A, Witherspoon F D, Case A, Luna M, Cassibry J, Vyas A & Gilmore M A, *Phys Plasmas*, 31 (2024) 102701.
16 Slutz S A & Vesey R A, *Phys Plasmas*, 29 (2023) 012708.
17 Gomez M R, *et al.*, *Phys Plasmas*, 31 (2024) 032706.
18 Awe T J, *et al*., *Phys Rev Lett*, 131 (2023) 235101.
19 McBride R D, *et al*., *Phys Plasmas*, 30 (2023) 102705.
20 Perkins L J, Logan B G & Zimmerman G B, *Nucl Fusion*, 64 (2024) 044001.
21 Betti R & Hurricane O A, *Nat Phys*, 19 (2023) 162.
22 Schekochihin A A, *Annu Rev Astron Astrophys*, 62 (2024) 317.
23 Howes G G, *Nat Rev Phys*, 6 (2024) 112.
24 Yamada M, Yoo J & Jara-Almonte J, *Nat Rev Phys*, 5 (2023) 624.
25 Ji H, Forest C B & Fiksel G, *Phys Today*, 77 (2024) 42.
26 Cerri S S, Califano F & Jenko F, *Phys Plasmas*, 31 (2024) 080501.
27 Matthaeus W H, Parashar T N & Shay M A, *Phys Plasmas*, 30 (2023) 032306.
28 Sironi L & Beloborodov A M, *Astrophys* J, 942 (2023) 102.
29 Walsh C A, Strozzi D J, Sio H, Pollock B B, Appelbe B D, Crilly A J, O'Neill S, Weber C, Chittenden J P & Moody J D, *High Energy Density Phys*, 51 (2024) 101103.
30 Pacific Fusion Scientific Collaboration, *MagLIF Ignition Studies for Pulsed-Power Fusion Systems*, APS-DPP 2025, American Physical Society Division of Plasma Physics Meeting.